SKELETAL ANATOMY IN THE YUCATAN MINIPIG CARPUS

By

Sophia Sordilla

ScB in Biology, Brown University, 2022

Thesis

Submitted in partial fulfillment of the requirements for the Degree of Master of Science in the Graduate Program of Biotechnology at Brown University

PROVIDENCE, RHODE ISLAND

FEBRUARY 2024

AUTHORIZATION TO LEND AND REPRODUCE THE THESIS

As the sole author of this thesis, I authorize Brown University to lend it to other institutions for the purpose of scholarly research.

Date_______________ _____________________________________
Sophia Sordilla, Author

I further authorize Brown University to reproduce this thesis by photocopying or other means, in total or in part, at the request of other institutions or individuals for the purpose of scholarly research.

Date_______________ _____________________________________
Sophia Sordilla, Author

This thesis by Sophia Sordilla is accepted in its present form by the Graduate Program in Biotechnology as satisfying the thesis requirements for the degree of Master of Science

Date_______________ Signature: ___________________________________

Dr. Joseph J. (Trey) Crisco, Advisor

Date_______________ Signature: ___________________________________

Dr. Sharon Swartz, Reader

Date_______________ Signature: ___________________________________

Dr. Elizabeth Brainerd, Reader

Approved by the Graduate Council

Date_______________ Signature: ___________________________________

Dr. Thomas Lewis, Dean of the Graduate School

Acknowledgments

First, I would like to thank my advisor Dr. Trey Crisco for his mentorship, guidance, and invaluable knowledge over the past year and a half. I'm very grateful to have had the opportunity to learn from him and grow as a researcher. I'm also grateful to all the other members of the lab for sharing their support and assistance. In particular, I'd like to thank Amy Morton and Quianna Vaughan for contributing their time, constructive criticism, and skillsets. Amy has spent numerous hours teaching me new concepts, techniques, and software. Quianna introduced me to the lab, helped me to collect data, and provided invaluable assistance in editing this document.

Second, I very much appreciate my thesis committee, Dr. Sharon Swartz and Dr. Elizabeth Brainerd, for contributing their time and extensive knowledge to this project. When I was an undergraduate, Dr. Swartz and Dr. Brainerd co-taught Human Anatomy and Biomechanics, which solidified my interest in the subject. I have very fond memories of lab sections in which we explored topics in both human and comparative anatomy. Additionally, Dr. Swartz mentored me as an undergraduate and has continued to support me throughout my graduate studies and beyond.

I'd also like to express my appreciation for my other mentors within academia. My program director, Dr. Jacquelyn Schell, introduced me to the Biotechnology master's program and has provided unwavering guidance over the past year and a half. I started working with Dr. Andrew Schulz as an undergraduate, and I'm extremely grateful for his mentorship over the years.

Finally, I'd like to thank the people who supported me outside of academics. My teammates have helped to shape the last five years of my life, supported me, and pushed me to improve at everything I do. The unwavering support of my friends and family has been invaluable throughout this program and in all my other pursuits.

Table of Contents

Table of Figures

Table of Tables

Abstract of Skeletal Anatomy in the Yucatan Minipig Carpus, by Sophia Sordilla, ScM in Biotechnology, Brown University, February 2024.

Objective: Osteoarthritis (OA) in the wrist can greatly decrease quality of life and is characterized by the degradation of soft tissues and the growth of osteophytes. Currently, there is a lack of viable treatment options for OA of the wrist compared to larger joints like the hip and knee. This is due in part to the lack of an established preclinical large animal model for the human wrist. Here, we conduct a holistic investigation into the carpal anatomy of the Yucatan minipig (YMP) to aid decisions about its viability as an animal model for wrist therapeutics.

Methods: Microcomputed tomography (µCT) and clinical computed tomography (CT) scans of the YMP carpal bones were used to measure and compare individual carpal bones within the YMP carpus to existing data on human carpal bones. Articular cartilage surface area and thickness were compared across YMP specimens and to human data. We conducted detailed dissections of the tendon and ligament anatomy of the YMP, focusing on analogues important to human carpal stability.

Results: YMP carpal bones were generally smaller in volume and surface area from human carpal bones. YMP carpal bones also differed from their human analogues in normalized volume, or the volume of the bone divided by the volume of the entire carpus. We found two specimens with abnormal carpal anatomy in which the first and second carpal bones were fused. Average articular cartilage thickness in the YMP radial carpal bone was 0.3 ± 14mm, markedly thinner than its human analogue, the scaphoid, at 0.8 ± 0.2mm. Flexor tendon anatomy had functional similarities to human anatomy, which was consistent with existing literature.

Conclusions: We found notable differences in carpal bone size and scaling, articular cartilage thickness and digital extensor tendon anatomy. Our anatomical findings may provide foundational information for other work seeking to use or considering the YMP as a preclinical animal model for carpal joint replacement and therapeutics.

Chapter 1: Introduction

Osteoarthritis (OA) in the wrist can cause pain and a reduced range of motion in the joint, decreasing quality of life and interfering with normal hand function [1]. This disease is characterized by the degeneration of tissues on articulating surfaces and the growth of bone spurs (osteophytes) on the edges of affected bones [2]. Noninvasive treatment options, including nonsteroidal and steroidal anti-inflammatory drugs, are generally the first course of treatment for a patient with OA. However, these drugs are used to alleviate the symptoms associated with OA instead of addressing the root condition [3]. More invasive treatment options to alleviate OA symptoms include surgical intervention such as immobilization of the joint (arthrodesis), removal of the osteoarthritic bone, and replacement of the joint with a prosthesis [4,5]. Although recent advancements have improved patient outcomes, prosthetic replacements for wrist joints have historically had high rates of complications in comparison to the larger joints. These complications include implant loosening, foreign body reactions, and patient pain [1,4]. Prosthetic replacement of single bones using first-generation silicone implants has been of interest due to the potential advantage of preserving native anatomical structures. However, silicone spacers have largely been abandoned due to high rates of complications, including dislocation and synovitis. Further inquiries have been made into alternate materials to address these modes of complication; these materials include pyrocarbon, titanium alloy, cobalt chrome, and patient-specific carpal bone replacement made from thermoplastic polymers like polyetheretherketone [1,6–9]. Standardized evaluation methods, including preclinical animal models, will be important to further developing and approving new orthopedic devices and materials for the wrist.

A significant barrier to the further development of wrist replacement technologies is the lack of a validated large animal model for preclinical study. Large animal models are particularly important for investigating therapeutics in which the device will encounter environments with mechanical loading [10]. According to the U.S. Food and Drug Administration's (FDA) Orthopedic Devices Program, a major regulatory gap in the approval of innovative orthopedic devices is the lack of established methods of validating such devices, including pre-clinical and computational models [11]. Joint replacement technology in larger joints, such as the hip and knee, have made great progress due to larger market size and the relative simplicity of these joints [12–14]. However, there is a smaller market size and no standard, validated animal model for new carpal bone and joint replacement technologies for the wrist.

Recent work has suggested the Yucatan minipig (YMP) as a useful preclinical animal model for orthopedic devices. The YMP is a small breed of domesticated pig that is relatively accessible to acquire and less expensive to keep than traditional domestic breeds, due to their smaller size [15]. The YMP has been recognized by the FDA as a relevant large animal model for spine-related indications, and further works have discussed this breed as a suitable model for trauma-induced osteoarthritis, lumbar facet joint cartilage, knee mechanics, cartilage healing, and forelimb flexor tendons [16–21].

However, comparatively less work has investigated the YMP as a model for carpal bone and joint replacement. Porcine forelimb anatomy has marked morphological differences from the human forelimb, but the skeletal anatomy is well conserved. All but one bone in the human carpus, the first metacarpal, has a porcine analogue (Figure 1). In 2021, Stoeckl et al. found that the accessory carpal bone (ACB) in the YMP was sufficiently similar in size, shape, and loading to the human trapezium carpal bone to be used as a model for joint replacement and resurfacing [3]. Additionally, a 2015 study by Behrends et al. found that the YMP was a suitable model for scaphoid fractures, non-unions, and repairs [22]. The YMP radial carpal bone (RCB) is analogous to the human scaphoid and similar in location, geometry, and blood supply [22]. Although the goal of this study is to generate holistic data about the YMP carpus, we have an added focus on the RCB due to its relevance as a model for the human scaphoid.

This study aims to provide a holistic characterization of the Yucatan mini pig carpal anatomy to better understand its potential as a preclinical animal model for carpal joint arthroplasty technologies. Through characterizing relevant tendons, ligaments, carpal bones, and articular cartilage, we aim to provide basic morphological data to compare the Yucatan mini pig to human carpal anatomy and investigate the role of individual variation in the breed.

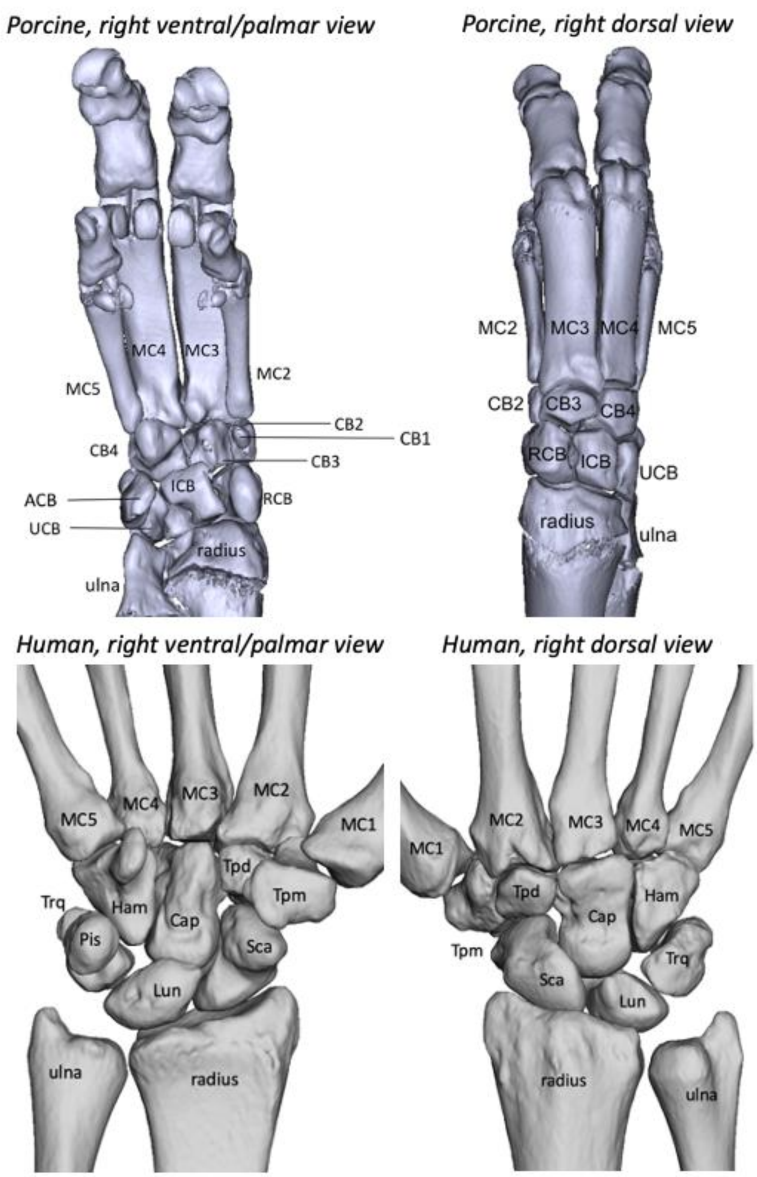

Human	Minipig
Metacarpals 2-5 (MC2-5)	Metacarpals 2-5 (MC2-5)
First metacarpal (MC1)	None
Trapezium (Tpm)	1st carpal bone (CB1)
Trapezoid (Tpd)	2nd carpal bone (CB2)
Capitate (Cap)	3rd carpal bone (CB3)
Hamate (Ham)	4th carpal bone (CB4)
Scaphoid (Sca)	Radial carpal bone (RCB)
Lunate (Lun)	Intermediate carpal bone (ICB)
Triquetrum (Trq)	Ulnar carpal bone (UCB)
Pisiform (Pis)	Accessory carpal bone (ACB)

Figure 1. Skeletal anatomy in the human (bottom) and porcine (top) carpi differ in morphology, however, nearly all bones in the human wrist have a porcine analogue.

Chapter 2: Methods

Specimens

Fourteen total YMP forelimb specimens were used to investigate anatomy, and one Yorkshire pig forelimb was used for a preliminary soft tissue dissection (Table 1). Microcomputed tomography (µCT) scans of all carpal bones from YMP forelimb specimen were used to investigate bony anatomy and articular cartilage (Specimen 1, or S1). Clinical computed tomography (CT) scans of eleven additional YMP forelimb specimens were used to investigate the role of individual variation in bony anatomy (S3-13). Additionally, µCT scans of the RCBs from these eleven forelimbs were used to investigate individual variation in articular cartilage (S3-13).

Two forelimbs, one YMP and one Yorkshire, were dissected to investigate tendon and ligament anatomy (S2 & S14). Specimens were kept frozen at -20°C from harvest until use. Before dissection or CT scanning, specimens were thawed at room temperature for 24 hours.

Table 1. Study specimens. B + AC denotes 'Bony anatomy and articular cartilage analysis.' RCB denotes 'radial carpal bone,' which is analogous to the human scaphoid.

Specimen ID	Species	Specimen Description	Procedure	Age (months)	Sex	Weight (kg)	Left/ Right
S1	Yucatan	Eight carpal bone µCTs	B + AC	19	F	55.9	R
S2	Yucatan	Intact Forelimb	Soft tissue dissection	20	F	60.0	L
S3	Yucatan	Forelimb CT, RCB µCT	B + AC	19	F	55.1	L

S4	Yucatan	Forelimb CT, RCB µCT	B + AC	18	F	49.8	L
S5	Yucatan	Forelimb CT, RCB µCT	B + AC	18	F	51.6	L
S6	Yucatan	Forelimb CT, RCB µCT	B + AC	18	F	56.1	L
S7	Yucatan	Forelimb CT, RCB µCT	B + AC	18	F	49.4	L
S8	Yucatan	Forelimb CT, RCB µCT	B + AC	18	F	50.6	L
S9	Yucatan	Forelimb CT, RCB µCT	B + AC	13	M	61.0	R
S10	Yucatan	Forelimb CT, RCB µCT	B + AC	18	F	55.1	R
S11	Yucatan	Forelimb CT, RCB µCT	B + AC	18	F	49.8	R
S12	Yucatan	Forelimb CT, RCB µCT	B + AC	18	F	49.4	R
S13	Yucatan	Forelimb CT, RCB µCT	B + AC	18	F	50.6	R
S14	Yorkshire	Intact Forelimb	Soft tissue dissection	5	F	46.7	L

Data Collection

Bony Anatomy

All eight S1 carpal bones and the RCBs from S3-S13 were resected and scanned using a MicroCT40 desktop μCT system (Scanco Medical, Brüttisellen CH). The system was set to 70KVp and 114 μA, and an isometric voxel size of 30 μm. The image files were converted to DICOM and exported for analysis in Mimics (Materialise, Leuven, BE). The individual carpal bones were segmented from the μCT images using an intensity threshold value of 2200 and manually edited to remove artifacts [23,24].

All YMP forelimb specimens (S1-S13) were imaged following the procedure described in Badida et al., 2020 using a clinical CT scanner (HighSpeed Advantage 16, GE, Milwaukee WI) [25]. These image files were exported for analysis in Mimics, and all carpal bones were segmented from the CT images using a lower intensity threshold value of 828. Carpal bones were then manually delineated from one another and edited to remove artifacts [23,24].

Articular Cartilage

For each carpal bone in S1 and the RCBs from S3-13, articular cartilage surface models were generated following the method described by Moore et al. for generating cartilage surfaces from μCT imaging of human carpal bones [26]. Articular cartilage was segmented using two different methods - manually in Mimics, and semi-automatically using both Mimics and Geomagic Wrap. To confirm precision and reproducibility of both manual and semi-automatic segmentation methods, we used each method to segment the S1 RCB three times.

Articular cartilage thickness, defined as the distance between the articular cartilage and subchondral bone meshes, was calculated using the open-source mesh generation toolbox iso2mesh (Version 1.9.5; Fang, 2020) in MATLAB (R2021a; Mathworks, Natick MA) [27]. Mean articular cartilage thickness and standard deviation were calculated for each carpal bone. Articular cartilage thickness was compared between carpal bones using the S1 samples, between individuals using the 11 collected RCBs, and to human carpal bone articular cartilage data from existing literature.

Tendon and Ligament Dissections

To investigate tendon and ligament anatomy, layer-by-layer dissections were performed on a Yorkshire pig and YMP forelimb (S2 and S14). Tendon and ligament attachment sites on each of the carpal bones were carefully located and confirmed. The prominent flexor and extensor tendons (radial extensor, extensor, radial and ulnar flexors) of the carpus were identified and insertion points were documented [28]. Any remaining tendons with insertion points on the carpal bones or digits were photographed and recorded. These findings were compared to existing documentation in veterinary textbooks and literature [29,30].

Ligament dissection was guided by previous literature identifying ligament divisions that cause carpal instability in humans, with a goal of identifying any existing analogues to these ligaments in the porcine carpus [31]. Ligaments were documented, photographed, and compared to human anatomy.

Data Analysis and Statistics

For the S1 carpal bones, centroid, surface area, and principal axes of inertia (assuming all bones had homogeneous density) were calculated using custom-written code in MATLAB [32–34]. Volume was calculated from the bone surface models using *Volume of a Surface Triangulation* (1.0.0; Suresh, n.d.). For each S1 carpal bone, normalized carpal bone volume (the volume of the individual carpal bone divided by the total volume of all carpal bones) was calculated using custom-written code in MATLAB.

For the 11 RCB µCTs (S1, S3-13), mean articular cartilage thickness and standard deviation were calculated for the proximal and distal facets using custom-written code in MATLAB. Additionally, a two-tailed student's t-test was used to compare cartilage thickness between the distal and proximal facets on the RCBs.

To compare semi-automatic and manual cartilage segmentation, we segmented the S1 RCB three times with each method. Descriptive statistics, including mean articular cartilage thickness and standard deviation, were generated for each cartilage segmentation trial. Articular cartilage thickness values generated by the semi-automatic trials were compared using an ANOVA. The three semi-automatic trials were statistically significant from one another, however, the mean articular cartilage thickness varied by only 0.02mm (Figure 2).

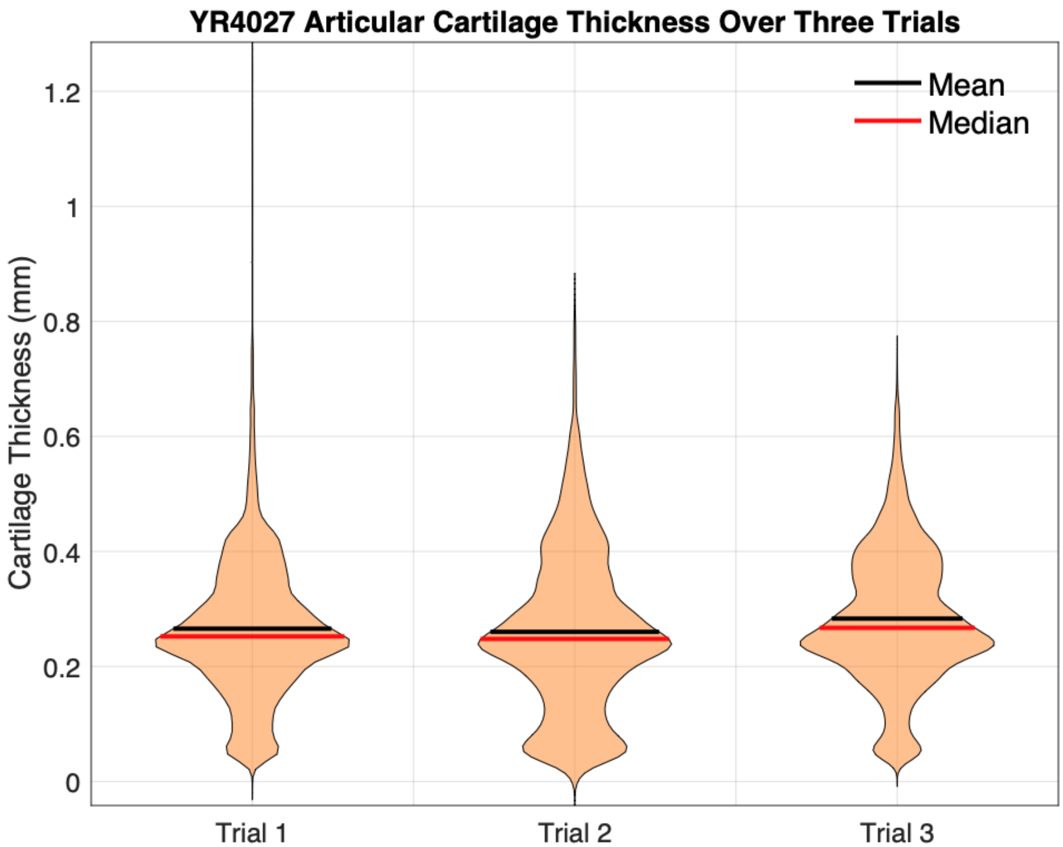

Figure 2. Mean articular cartilage thickness for each trial varied by 0.2 mm, with the first trial having the most outliers.

Chapter 3: Results

Bony Anatomy

The YMP carpus is composed of eight individual carpal bones. Each of the carpal bones has a human carpal bone analogue with the articulations between the carpals conserved. These carpal bones form two rows articulating proximally with the radius and ulna, and distally with the four metacarpals (Figure 1). In the proximal row, the radial carpal bone (RCB) sits the furthest medially and is analogous to the human scaphoid. Laterally, the RCB articulates with the intermediate carpal bone (ICB), which is analogous to the human lunate. Lateral to the ICB is the ulnar carpal bone (UCB), which sits the furthest laterally in the proximal row and is analogous to the triquetrum. Volar to the UCB is the accessory carpal bone (ACB), which is analogous to the pisiform.

Furthest medially in the distal carpal row are the first and second carpal bones (CB1 and CB2). CB1 is analogous to the human trapezium and articulates on the volar side of CB2, which is analogous to the trapezoid. Lateral to CB2 is the third carpal bone (CB3), analogous to the capitate, and the fourth carpal bone (CB4) sits the furthest laterally in the distal carpal row and is analogous to the hamate.

One notable difference of porcine anatomy relative to human anatomy is the lack of a first digit (first metacarpal, proximal and distal phalanges), or thumb, in the porcine carpus. The first carpal bone in the porcine carpus, analogous to the trapezium, is also reduced in volume. Additionally, the radius and ulna of the YMP are fused, limiting range of motion in supination and pronation as compared to humans.

Bone Volume and Surface Area

S1 Carpal bones

The eight S1 carpal bones differed in surface area and volume. Carpal bone surface area ranged from 90mm^2 on CB1 to 904mm^2 on the ICB. Volume ranged from 60mm^3 (CB1) to 1705mm^3 (ICB). The largest carpal bone by both volume and surface area was the ICB, followed by CB4, the RCB, CB3, the UCB, the ACB, CB2, and CB1 (Table 2). This order remains the same for normalized volume, with the ICB making up 20.4% of the total volume of the carpus.

Table 2. Surface area and volume of the S1 carpal bones.

	CB1	CB2	CB3	CB4	ACB	ICB	RCB	UCB
Surface area (mm^2)	90	246	669	863	501	904	805	669
Volume (mm^3)	68	267	1166	1689	721	1705	1584	1159

Variation between individuals (S3-13)

Mean carpal bone volumes for the forelimb CT specimens (S3-13) followed the same size trends as described above for S1 (Figure 3).

Notably, two forelimb specimens (S8 and S13) did not have a distinct CB1 and CB2. Instead, these bones appeared to be fused with no visible delineation in the CT scans (Appendix C). These specimens were processed as having no CB1 (volume of 0 mm^3), and the fused bones were included in the mean CB2 volume. Inclusion of these specimens did not change the trends observed but increased the mean volume of CB2 by 9.9 mm^3 (from 275.6 mm^3 to 285.5 mm^3).

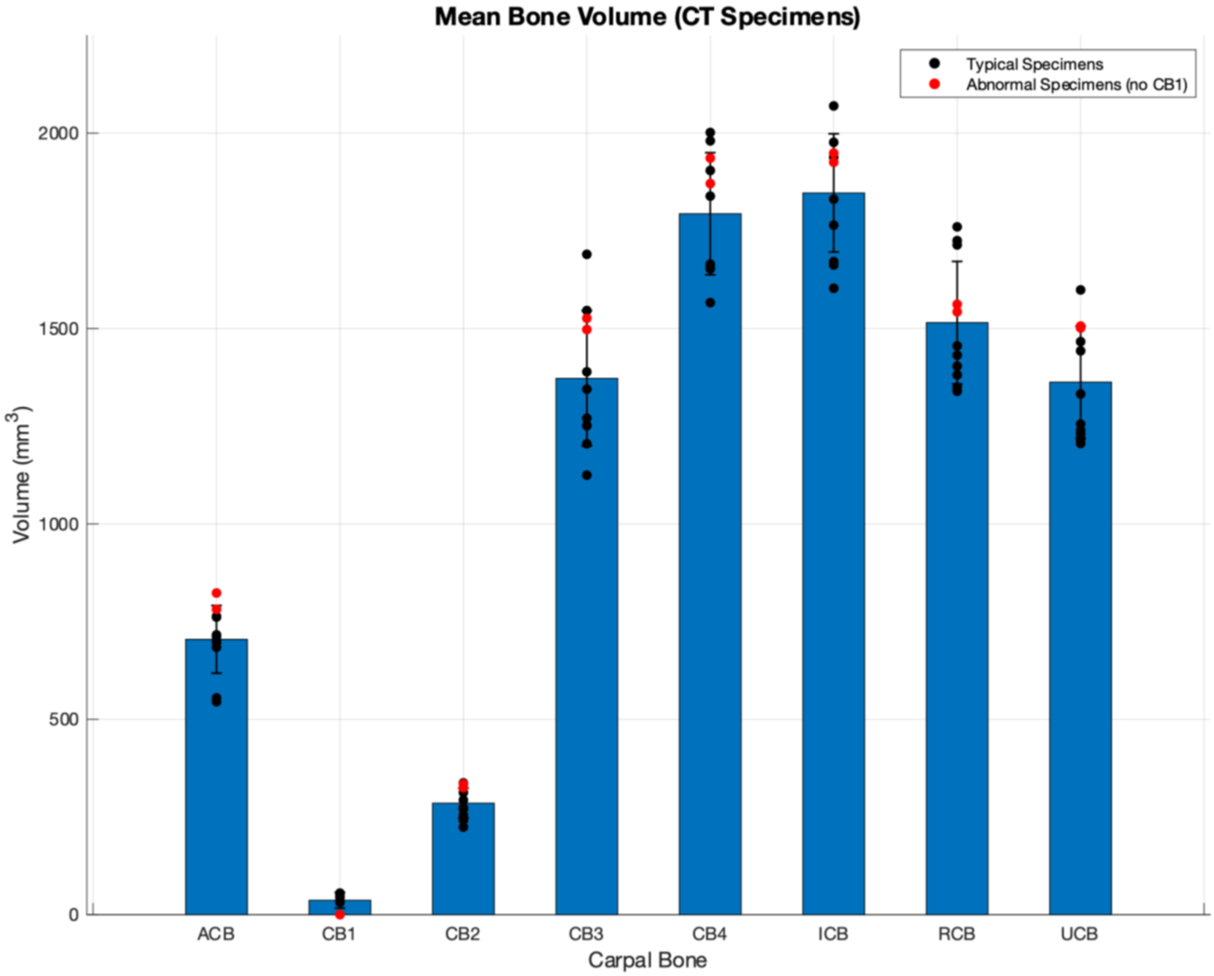

Figure 3. Mean bone volume by carpal bone for S3-13 (S8 and S13, in which CB1 and CB2 were fused, are represented in red).

Articular Cartilage

Within the S1 carpal bones, average articular cartilage thickness varied between 0.2mm (CB1) and 0.4mm (ACB) (Table 3, Appendix B). Additionally, cartilage thickness varied across each articular facet (Figure 4).

Table 3. Descriptive statistics of S1 articular cartilage thickness by carpal bone.

	CB1	**CB2**	**CB3**	**CB4**	**ACB**	**ICB**	**RCB**	**UCB**
Average (mm)	0.15	0.29	0.23	0.27	0.38	0.22	0.27	0.33
Standard Deviation (mm)	0.07	0.20	0.08	0.09	0.10	0.11	0.12	0.10

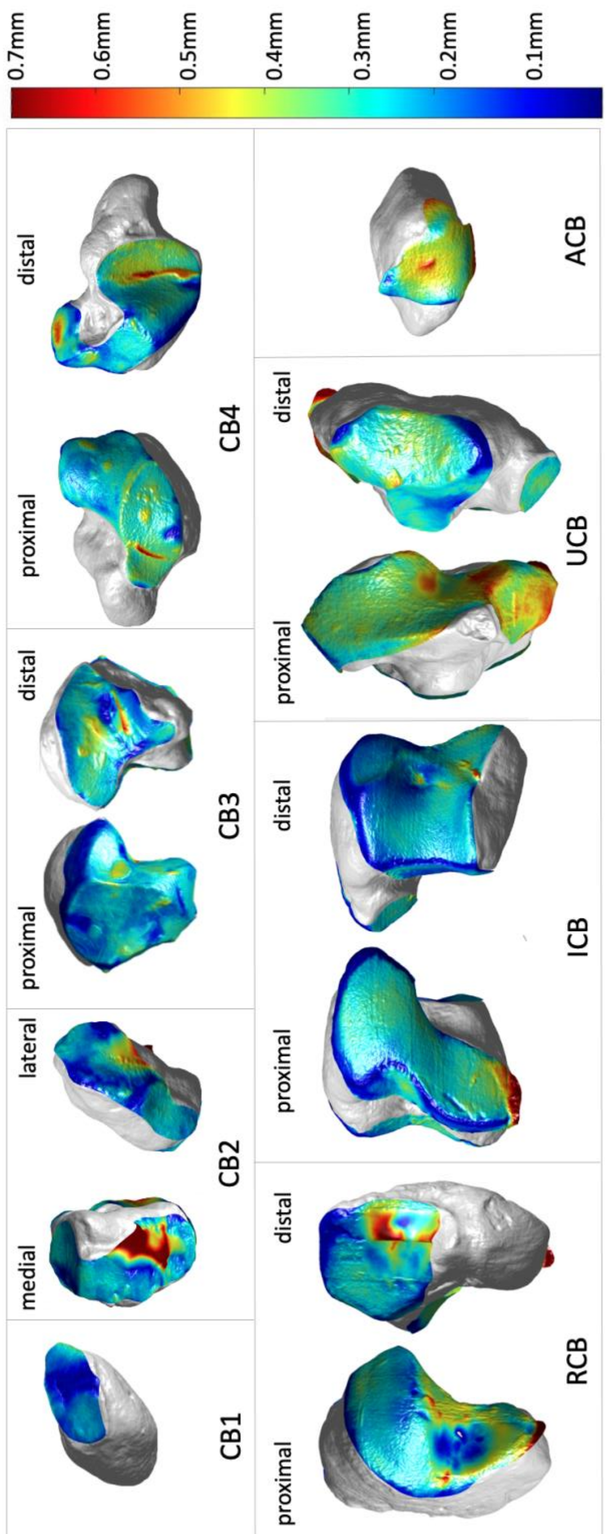

Figure 4. Heatmaps of articular cartilage thickness in S1 carpus (carpal bones not to scale).

Mean articular cartilage thickness for the 11 RCB specimens was 0.3±0.03 mm for the distal facet and 0.3±0.04 mm for the proximal facet. A two-tailed t test found no significant differences between cartilage thickness on the distal and proximal facets using a p value of 0.05 ($p = 0.090$). Overall, articular cartilage thickness ranged from 0.2 mm to 0.4 mm (Figure 5).

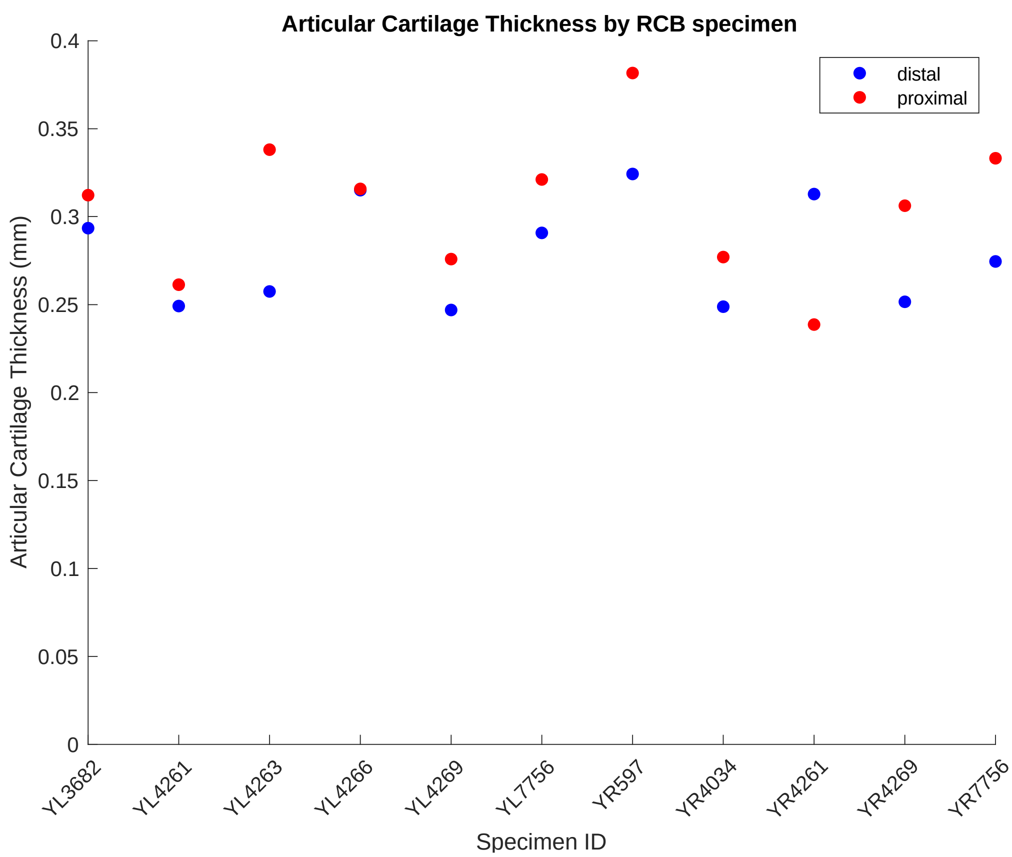

Figure 5. Articular cartilage thickness by RCB specimen and facet (red = proximal, blue = distal).

Tendon Dissection

Tendons were categorized as flexors or extensors based on location of insertion. The extensor tendons inserted on the dorsal side of the carpus to enable extension of the digits and the wrist. Immediately deep to the skin and fascia, several superficial tendons originating at the humerus inserted dorsally on the digits. The lateral digital extensor tendon branches to insert on the proximal ends of the 4th and 5th phalanges. Another broad, superficial digital extensor inserts distally at the 4th phalanx. The common digital extensor runs superficially along the dorsal midline of the forelimb and inserts distally on the 3rd and 4th phalanges. Deep to the first layer of tendons are two relatively broad carpal extensor tendons. The radial extensor of the carpus runs along the medial side of the carpus, enveloping the first carpal bone and inserting on the proximal second metacarpal and second carpal bone. The other extensor of the carpus runs anterior and branches distally to insert on the proximal ends of the 3rd and 4th metacarpals (Figure 6).

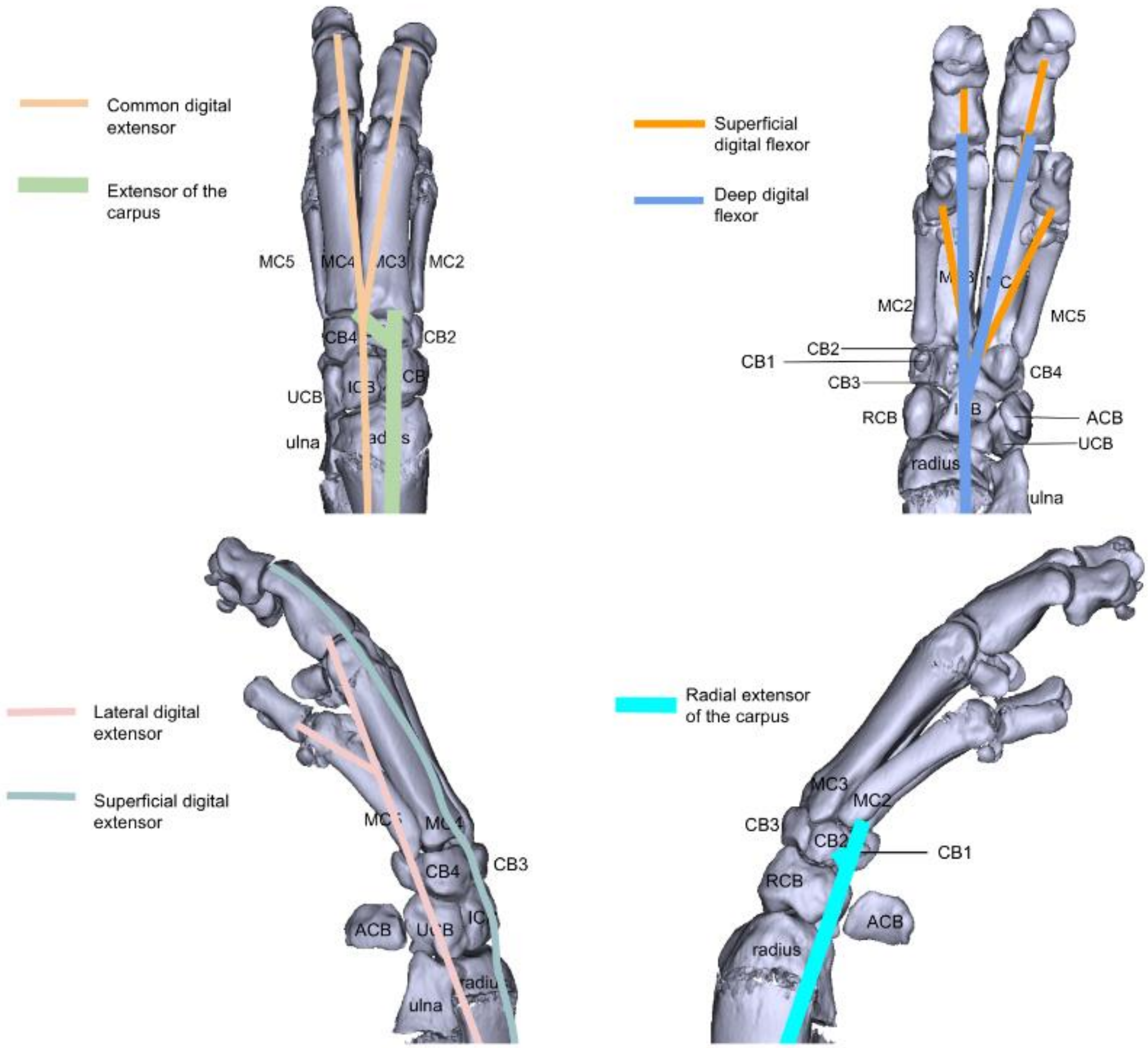

Figure 6. Clockwise: dorsal, volar, radial, and ulnar renderings of tendon anatomy on the YMP carpus. Dorsal extensor tendons on the YMP carpus.

Flexor tendons inserted on the volar side of the carpus on the metacarpals and phalanges. The forelimb flexor tendons were bound together by connective tissue on the volar side of the carpus, and branch distally to insert on the metacarpals and phalanges (Figure 7). Two digital flexor tendons originate at the humerus. The superficial digital flexor branches distally and inserts on the proximal ends of the 3rd and 4th phalanges. The superficial digital flexor envelopes the deep digital flexor, which inserts at the distal end of each phalanx. Additionally, the superficial ulnar flexor of the carpus inserted on the ACB and the proximal end of the fifth metacarpal.

Figure 7. Volar view of the left YMP forelimb. The volar flexor tendons are held in place by a band of connective tissue (arrow).

Chapter 4: Discussion and Conclusions

Invasive treatments that address the root causes of carpal osteoarthritis have experienced limited progress, in part due to the lack of an established preclinical animal model. In this work we investigated the articular cartilage, tendon, and bony anatomy of the Yucatan mini pig carpus in order to aid evaluations of its suitability as a model for the human wrist.

Bony Anatomy

Comparisons between our data on the YMP and existing literature on human carpal bones showed differences in volume (Figure 8). On average, human carpal bone volumes were larger than their porcine analogues in all carpal bones, except for the lunate and triquetrum. YMP RCB volumes averaged 1,827 ± 161.5 mm^3, while a previous study found that the analogous human carpal bone, the scaphoid, has an average volume of 2390.1 ± 673.6 mm^3 [32].

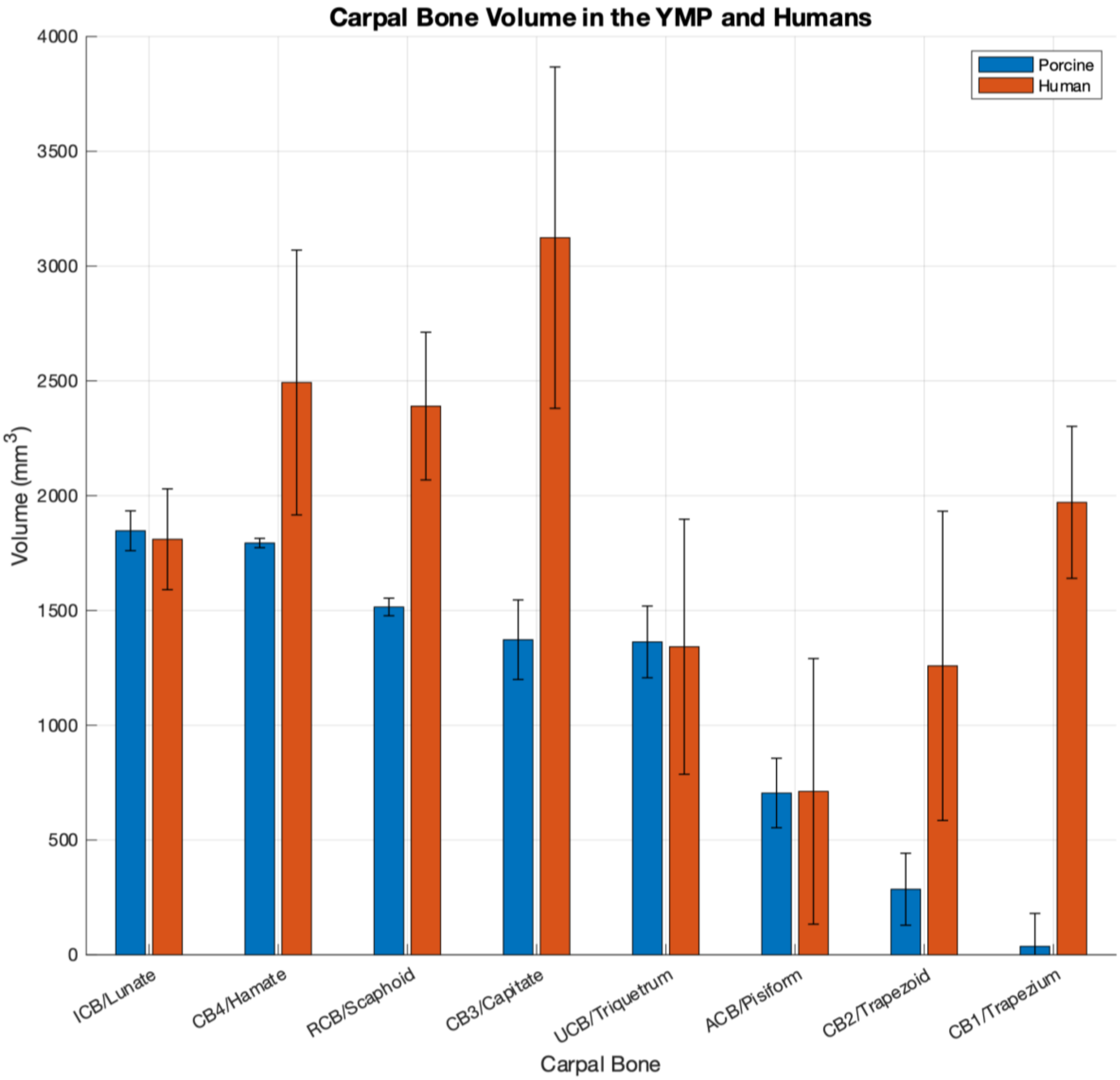

Figure 8. Gross volume of each carpal bone for the YMP (blue) and humans (red).

In comparing normalized carpal bone volumes (the volume of the individual carpal bone divided by the total volume of all carpal bones), the rank order of human carpal bone volumes and their porcine analogues differed (Figure 9). In humans, the largest carpal bone by normalized volume is the capitate, followed in descending order by the hamate, scaphoid, trapezium, lunate, triquetrum, trapezoid, and pisiform. In our YMP dataset, the largest carpal bone by volume was analogous to the lunate, followed by the hamate, scaphoid, capitate, triquetrum, pisiform, trapezoid, and trapezium.

In other words, normalizing for the volume of the carpus showed that human and porcine carpal bones were not isometrically scaled versions of one another. These results suggest an allometric scaling relationship between the YMP and human carpal anatomy.

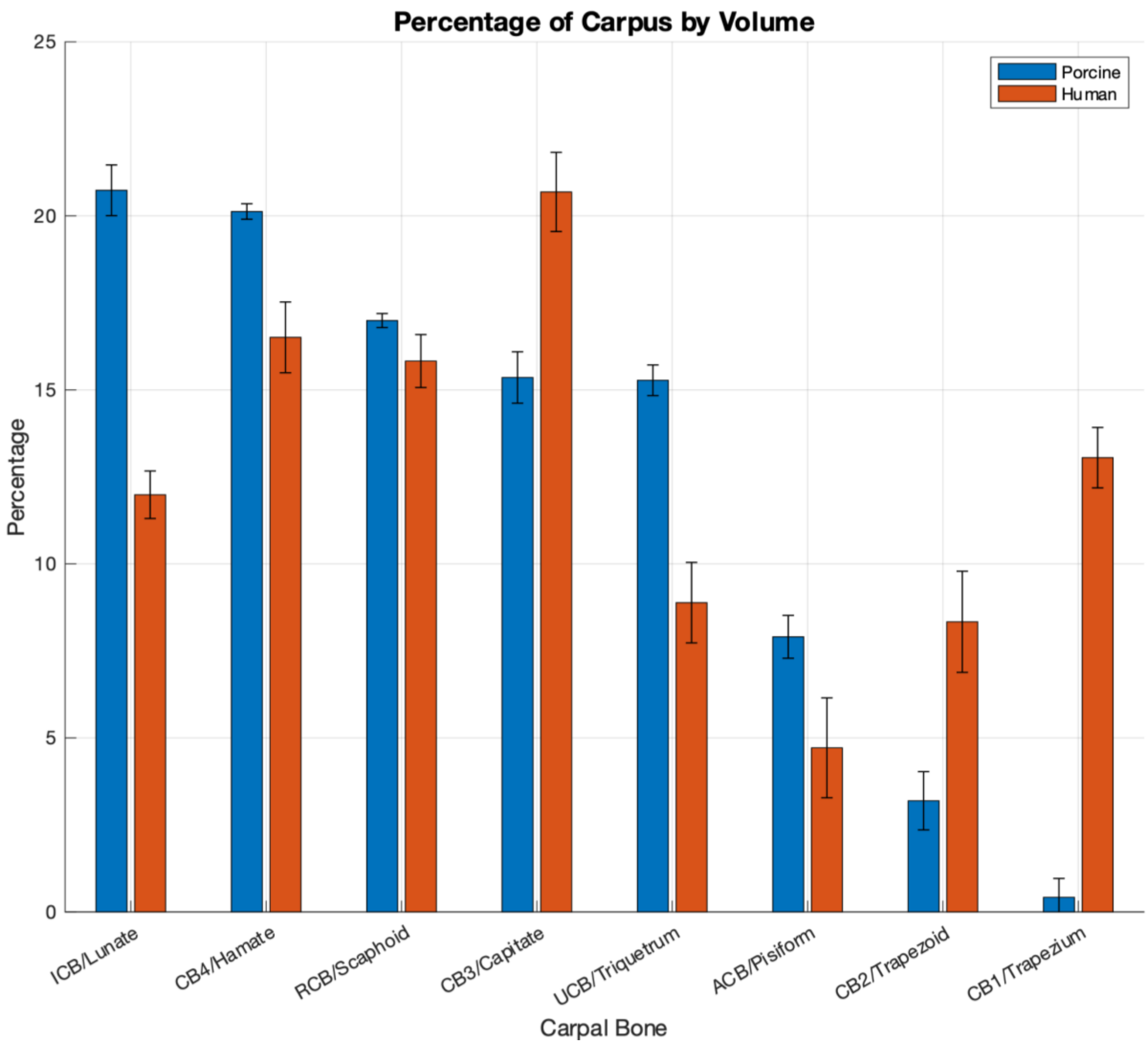

Figure 9. Relative volume of each carpal bone for the YMP (blue) and humans (red), calculated as the volume of the carpal bone divided by the total volume of the carpus.

During our analysis, we found that two of the eleven forelimb specimens (S8 and S13) had abnormal anatomy in which the first and second carpal bones were fused together (Appendix B). In contract to its human analogue, the trapezium, CB1 does not typically articulate with any metacarpal and does not serve a function in the porcine carpus. These two outlying specimens may have a fused CB1 and CB2 because CB1 is a vestigial structure and there is no selective pressure on the bone. Further study with larger sample sizes could illuminate the frequency with which this atypical anatomy occurs.

Articular Cartilage

Comparisons of articular cartilage thickness between carpal bones showed variation within the S1 carpus, and results were similar to existing literature on the YMP. Between the S1 carpal bones, average articular cartilage thickness had a range from 0.2mm to 0.4mm. CB1 had the thinnest average cartilage, followed by the ICB, CB3, RCB, CB4, CB2, UCB, and ACB. Existing literature on YMP cartilage was limited, but a 2021 study focusing on the ACB found that the articular cartilage ranged from 0.4mm to 0.5mm, with the thickest cartilage in the center of the facet [3]. Our methods yielded similar results, with the ACB cartilage averaging 0.4mm with some of the thickest cartilage in the center of the articular surface.

There was relatively little variation between individual RCB specimens and between the distal and proximal facets. Average articular cartilage thickness on the distal facets was 0.28mm and proximal facets averaged 0.31mm, with no statistically significant difference between the locations ($p = 0.090$). The mean articular cartilage thickness values had a range of 0.14 mm. This range of average thickness values between RCB specimens suggests that articular cartilage thickness is relatively consistent across individuals. In direct comparison, human articular cartilage is notably thicker. The RCB is analogous to the human scaphoid, which has been found to have an average articular cartilage thickness of 0.847 ± 0.174mm using similar methods to our study [26].

Tendon Anatomy

Tendon anatomy in the Yucatan and Yorkshire specimens was consistent with existing literature on the porcine carpus [21,29]. Further, our findings agreed with conclusions drawn by previous studies, in that porcine flexor tendon anatomy was similar to human flexor tendons [30]. YMP flexor tendons consisted of the deep digital flexor enveloped by the superficial digital flexor, held in place by connective tissue. This enveloping relationship is similar to human digital flexors (*flexor digitorum superficialis* and *flexor digitorum profundus*).

The human digital extensors consist of the *extensor digitorum*, which originates on the humerus and inserts on digits 2-5, and the *extensor digitorum minimi*, which inserts on the proximal end of the 5th phalanx. This differs from the digital extensors found in the YMP, which only insert on the center two digits (common digital extensor) and digits 4 and 5 (lateral digital extensor). The deep YMP extensor tendons had similar origin and insertion sites to their human analogues. The porcine radial extensor of the carpus was consistent with its human analogue, the *extensor carpi radialis longus*, which originates on the humerus and inserts on the second metacarpal. Additional extensors found in the carpus inserted on both the third and fourth metacarpals, similar to the *extensor carpi radialis brevis*, which inserts only on the third metacarpal.

Limitations

This study is primarily limited by constraints on specimen availability. Previous work on human carpal bone shape and size have suggested that bone volume is influenced by the sex of the individual[32]. However, our sample of YMP forelimbs included only one forelimb from a male specimen. Therefore, we did not conduct any analyses on the role of sex in YMP carpal bone size and scaling.

Only one complete set of eight carpal bones, S1, was used to generate data on articular cartilage throughout the carpus. However, our analysis of 11 YMP RCBs may provide insight into the role of individual variation. For the RCBs, articular cartilage thickness values all fell within a 0.14 mm range, indicating that other YMP individuals may not differ much from the S1 results.

Only one Yucatan mini pig forelimb and one Yorkshire mini pig forelimb were used to examine tendon and ligament anatomy. Muscle bellies originated from the humerus, but the muscles were separated from the humerus during specimen collection so further detail on origination for tendons was not possible. This low sample size means that limited conclusions can be drawn from this study alone, as other Yucatan mini pig individuals could have varied anatomy. However, both the Yucatan and Yorkshire specimens had the same attachment points for soft tissue anatomy, which could imply that these attachment points are relatively conserved between porcine breeds and individuals. Additionally, these results were consistent with existing literature on porcine tendon anatomy, indicating further that this anatomy is conserved across individuals [29].

Another limitation of the present work is the level of precision of the semi-automatic segmentation methods, given that an ANOVA found statistically significant differences between repeated segmentations of the same bone. However, the segmentation methods are consistent with published work validating these methods [26]. Additionally, we showed that these repeated segmentation trials resulted in cartilage measurements within 0.02mm of one another. These results indicate that the segmentation methods produced meaningfully consistent results between specimens.

This work aims to provide anatomical data as a basis for evaluating the YMP as an animal model for therapeutics in the wrist. We found notable differences in carpal bone size and scaling, articular cartilage thickness, digital extensor tendon anatomy, and volar ligament anatomy. Our anatomical findings may provide foundational information for other work seeking to use or considering the YMP as a preclinical animal model for carpal joint replacement and therapeutics.

References

1. Lerebours A, Marin F, Bouvier S, Egles C, Rassineux A, Masquelet AC. Trends in Trapeziometacarpal Implant Design: A Systematic Survey Based on Patents and Administrative Databases. *J Hand Surg*. 2020;45(3):223-238. doi:10.1016/j.jhsa.2019.11.015

2. NIAMS Science Communications and Outreach. Osteoarthritis. National Institute of Arthritis and Musculoskeletal and Skin Diseases. Published April 7, 2017. Accessed July 20, 2023. https://www.niams.nih.gov/health-topics/osteoarthritis

3. Stoeckl BD, Zlotnick HM, Farrell MJ, et al. The porcine accessory carpal bone as a model for biologic joint replacement for trapeziometacarpal osteoarthritis. *Acta Biomater*. 2021;129:159-168. doi:10.1016/j.actbio.2021.05.011

4. Eltorai AEM, Han A. Developments in trapezium Replacements. *Orthop Rev*. 2017;9(3):7196. doi:10.4081/or.2017.7196

5. Herren DB, Ishikawa H, Rizzo M, Ross M, Solomons M. Arthroplasty in the hand: what works and what doesn't? *J Hand Surg Eur Vol*. 2022;47(1):4-11. doi:10.1177/17531934211017703

6. Stratton-Powell AA, Pasko KM, Brockett CL, Tipper JL. The Biologic Response to Polyetheretherketone (PEEK) Wear Particles in Total Joint Replacement: A Systematic Review. *Clin Orthop Relat Res*. 2016;474(11):2394-2404. doi:10.1007/s11999-016-4976-z

7. Bæk Hansen T. Joint replacement for trapeziometacarpal osteoarthritis: implants and outcomes. *J Hand Surg Eur Vol*. 2021;46(2):115-119. doi:10.1177/1753193420917582

8. Honigmann P, Sharma N, Schumacher R, Rueegg J, Haefeli M, Thieringer F. In-Hospital 3D Printed Scaphoid Prosthesis Using Medical-Grade Polyetheretherketone (PEEK) Biomaterial. *BioMed Res Int*. 2021;2021:1301028. doi:10.1155/2021/1301028

9. ASM Medical Materials Database, http://mio.asminternational.org.revproxy.brown.edu/mmd/ Accessed December 2022.

10. Imwinkelried T, Beck S, Schaller B. Pre-clinical testing of human size magnesium implants in miniature pigs: Implant degradation and bone fracture healing at multiple implantation sites. *Mater Sci Eng C*. 2020;108:110389. doi:10.1016/j.msec.2019.110389

11. Health C for D and R. Orthopedic Devices Program: Research on Orthopedic Medical Devices. *FDA*. Published online March 24, 2021. Accessed January 17, 2023. https://www.fda.gov/medical-devices/medical-device-regulatory-science-research-programs-conducted-osel/orthopedic-devices-program-research-orthopedic-medical-devices

12. Grandview Research. Upper Extremity Implants Market Size & Share [2023 Report]. Accessed August 23, 2023. https://www.grandviewresearch.com/industry-analysis/upper-extremity-implants-market-report

13. Grandview Research. Knee Implant Market Size, Share & Growth Report, 2030. Accessed August 23, 2023. https://www.grandviewresearch.com/industry-analysis/knee-implants-market

14. Grandview Research. Hip Replacement Implants Market Size & Share Report, 2030. Accessed August 23, 2023. https://www.grandviewresearch.com/industry-analysis/hip-replacement-implants-market

15. Swindle MM, Makin A, Herron AJ, Clubb FJ, Frazier KS. Swine as Models in Biomedical Research and Toxicology Testing. *Vet Pathol*. 2012;49(2):344-356. doi:10.1177/0300985811402846

16. Nordberg RC, Kim AN, Hight JM, et al. Biochemical and biomechanical characterization of the cervical, thoracic, and lumbar facet joint cartilage in the Yucatan minipig. *J Biomech*. 2022;142:111238. doi:10.1016/j.jbiomech.2022.111238

17. Goetz JE, Fredericks D, Petersen E, et al. A clinically realistic large animal model of intra-articular fracture that progresses to post-traumatic osteoarthritis. *Osteoarthritis Cartilage*. 2015;23(10):1797-1805. doi:10.1016/j.joca.2015.05.022

18. O'Leary SA, Link JM, Klineberg EO, Hu JC, Athanasiou KA. Characterization of facet joint cartilage properties in the human and interspecies comparisons. *Acta Biomater*. 2017;54:367-376. doi:10.1016/j.actbio.2017.03.017

19. Han P fei, Zhang R, Gao Y yang, Li P cui, Wei X chun, Lv Z. Establishment and Simulation of 3D Geometric Models of Mini-Pig and Sheep Knee Joints Using Finite Element Analysis. *Med Sci Monit Int Med J Exp Clin Res*. 2020;26:e921540-1-e921540-12. doi:10.12659/MSM.921540

20. Pfeifer CG, Fisher MB, Saxena V, et al. Age-Dependent Subchondral Bone Remodeling and Cartilage Repair in a Minipig Defect Model. *Tissue Eng Part C Methods*. 2017;23(11):745-753. doi:10.1089/ten.tec.2017.0109

21. SMITH AM, FORDER JA, ANNAPUREDDY SR, REDDY KSK, AMIS AA. The Porcine Forelimb as a Model for Human Flexor Tendon Surgery. *J Hand Surg*. 2005;30(3):307-309. doi:10.1016/J.JHSB.2005.02.003

22. Behrends DA, Khendek L, Gao C, Zayed N, Henderson JE, Martineau PA. Characterization of a Pre-Clinical Mini-Pig Model of Scaphoid Non-Union. *J Funct Biomater*. 2015;6(2):407-421. doi:10.3390/jfb6020407

23. 3D Systems, Inc. Geomagic Wrap. https://oqton.com/geomagic-wrap/

24. Materialise. Materialise Mimics | 3D Medical Image Processing Software. Accessed June 5, 2023. https://www.materialise.com/en/healthcare/mimics-innovation-suite/mimics

25. Badida R, Garcia-Lopez E, Sise C, Moore DC, Crisco JJ. An Approach to Robotic Testing of the Wrist Using Three-Dimensional Imaging and a Hybrid Testing Methodology. *J Biomech Eng*. 2020;142(6):064501. doi:10.1115/1.4046050

26. Moore DC, Casey JA, Gilbert SL, Crisco JJ. μCT-GENERATED CARPAL CARTILAGE SURFACES: VALIDATION OF A TECHNIQUE. *J Biomech*. 2011;44(13):2516-2519. doi:10.1016/j.jbiomech.2011.06.027

27. Tran AP, Yan S, Fang Q. Improving model-based functional near-infrared spectroscopy analysis using mesh-based anatomical and light-transport models. *Neurophotonics*. 2020;7(1):015008. doi:10.1117/1.NPh.7.1.015008

28. Altieri MK. *The Feasibility of the Porcine Carpus as a Preclinical Biomechanical Animal Model of the Human Wrist for the Advancement of Novel Therapeutics*. Brown University; 2023. Accessed July 11, 2023. https://repository.library.brown.edu/studio/item/bdr:m34a85cm/

29. Konig HE, Liebach HG. *Veterinary Anatomy of Domestic Animals*. 7th ed.; 2020. DOI 10.1055/b-007-167437

30. Mao WF, Wu YF, Zhou YL, Tang JB. A study of the anatomy and repair strengths of porcine flexor and extensor tendons: are they appropriate experimental models? *J Hand Surg Eur Vol*. 2011;36(8):663-669. doi:10.1177/1753193411414117

31. Wolfe SW, Kakar S. Chapter 13: Carpal Instability. In: Wolfe SW, Pederson WC, Kozin SH, Cohen MS, eds. *Green's Operative Hand Surgery*. Eighth Edition. Elsevier Health Sciences; 2022.

32. Crisco JJ, Coburn JC, Moore DC, Upal MA. Carpal bone size and scaling in men versus in women. *J Hand Surg*. 2005;30(1):35-42. doi:10.1016/j.jhsa.2004.08.012

33. Suresh K. Volume of a surface triangulation. https://www.mathworks.com/matlabcentral/fileexchange/26982-volume-of-a-surface-triangulation

34. MATLAB. https://www.mathworks.com

35. Thorup VM, Laursen B, Jensen BR. Net joint kinetics in the limbs of pigs walking on concrete floor in dry and contaminated conditions1. *J Anim Sci*. 2008;86(4):992-998. doi:10.2527/jas.2007-0581

Appendix A

Ligament Dissection Results

On the dorsal side of the carpus, we identified nine ligaments connecting the carpal bones, metacarpals, radius, and ulna (Figure A1). The superficial radial intermediate ligament inserted on the RCB, ICB, and UCB, connecting the proximal carpal row. Additionally, the deep radial intercarpal ligament connects the ulnar face of the RCB with the radial side of the ICB. The dorsal intercarpal ligament inserted on the RCB, ICB, and the fourth carpal bone. Further connections were found between the UCB-CB3, RCB- ICB, UCB-ICB, UCB-radius, ICB-radius, and ICB-CB4. An additional ligament originated on CB3 and branched to the second and third metacarpals.

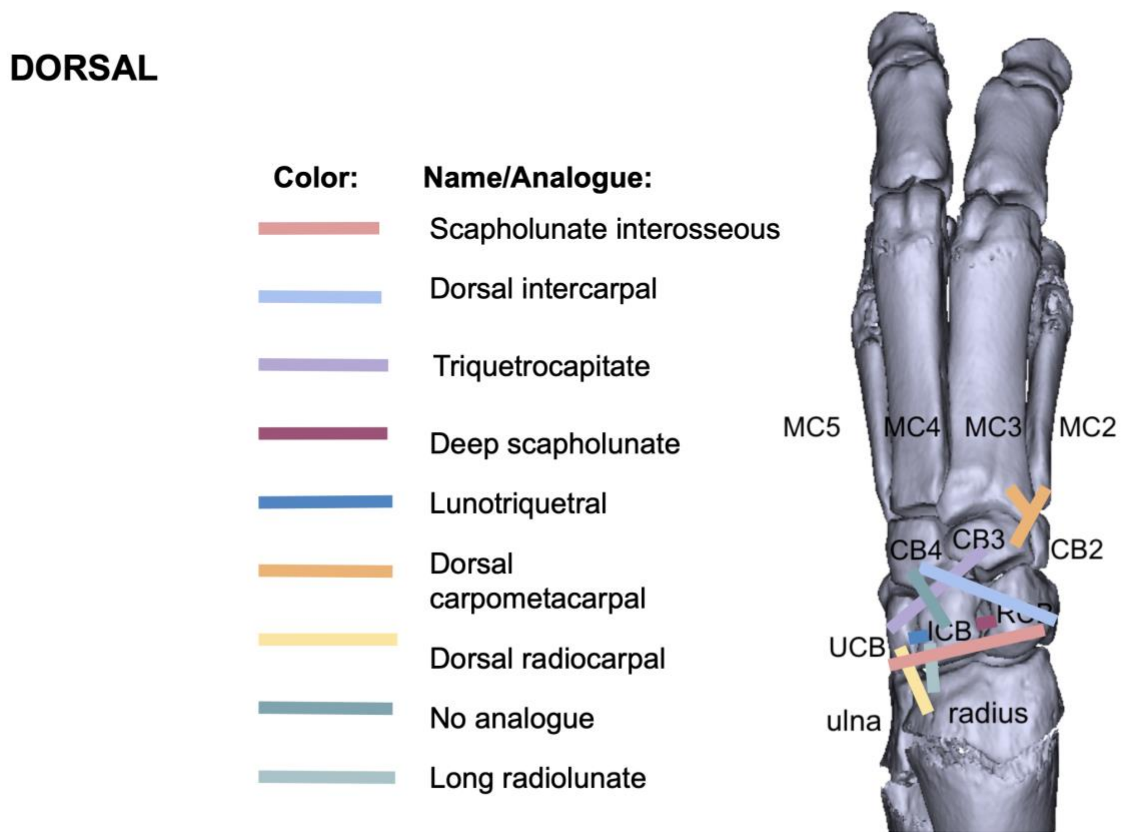

Figure A1. Dorsal ligaments found in the YMP carpus.

Radially, we found a ligament originating on the RCB that branched distally to insert on the first and second carpal bones (Figure A2).

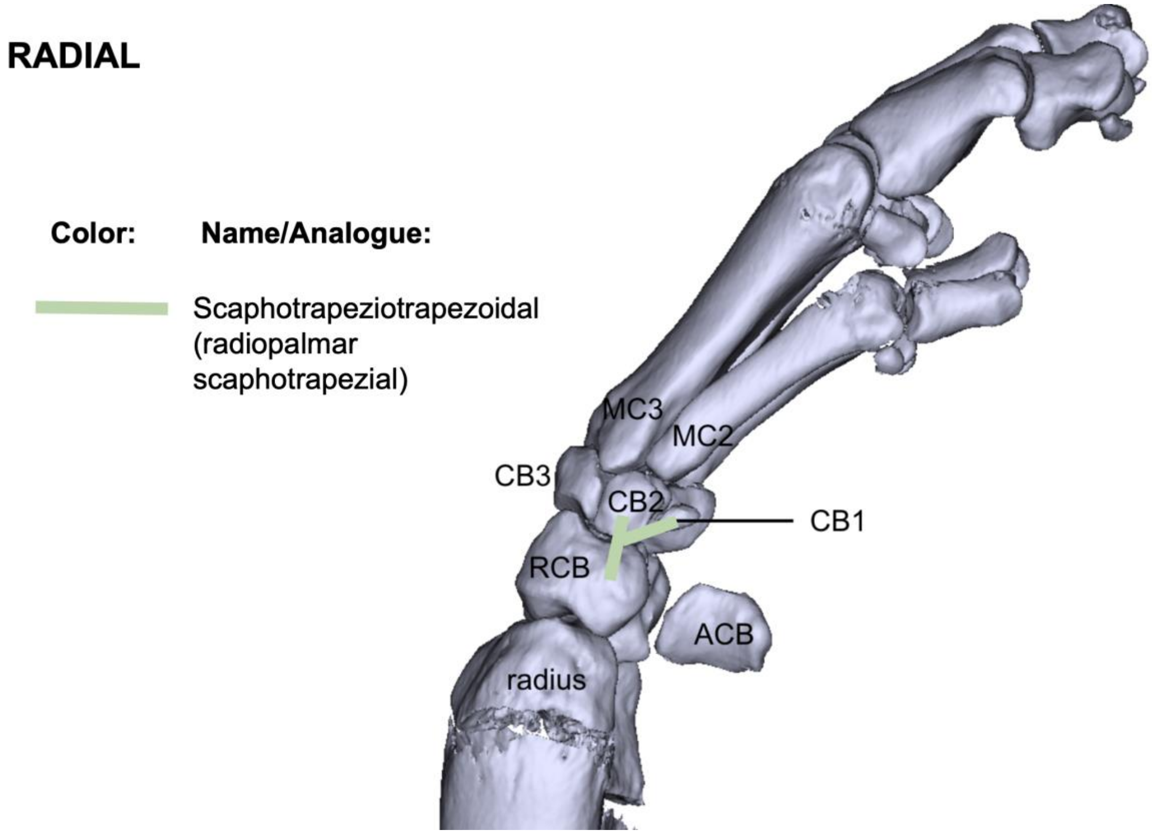

Figure A2. On the radial side, the YMP carpus contains an analogue to the human radiopalmar scaphotrapezial ligament.

The volar YMP ligaments were grouped into superficial and deep ligaments. In the superficial layer, ligaments connected the CB3-CB4, RCB-ICB, UCB-ICB, radius-RCB, radius-ACB, ulna-ICB, ulna-RCB, and ulna-UCB (Figure A3, top).

In the deep layer, one ligament originated on the ICB and branched distally to insert on CB3 and CB4. Another inserted on the radius and UCB. Additionally, we found ligaments attaching the radius-RCB-CB3, ulna-CB3, and UCB-CB4 (Figure A3, bottom).

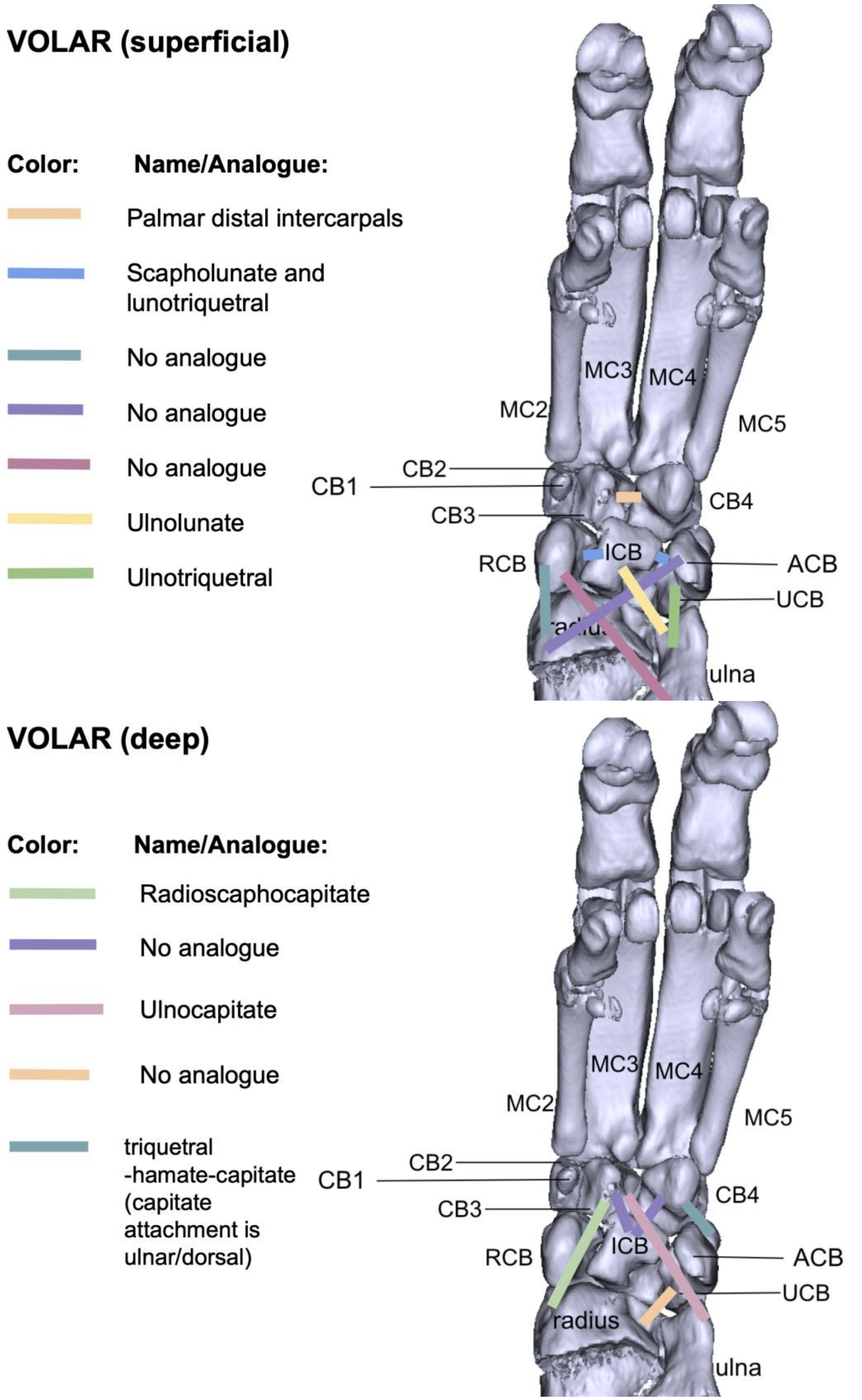

Figure A3. Superficial (top) and deep (bottom) volar ligaments in the YMP carpus.

Ligament Discussion

Ligament dissection revealed both similarities and differences between YMP and human forelimb anatomy. The dorsal side of the Yucatan wrist contained several analogues to ligaments important to carpal stability. These included the radial intermediate ligament, which connects the proximal carpal row and is analogous to the human scapholunate interosseous ligament, and the dorsal intercarpal ligament, which attaches the RCB and ICB to the fourth carpal bone [31]. Additionally, analogues were identified for the human triquetrocapitate, scapholunate, lunotriquetral, dorsal radiocarpal, and long radiolunate (Figure 5). One ligament, connecting the ICB (lunate) and fourth carpal bone (hamate), does not appear to have a human analogue.

Radially, we found a branching ligament connecting the RCB to the first and second carpal bones (Figure 6). This ligament is analogous to the radiopalmar scaphotrapezial ligament in humans.

Volar anatomy showed the most divergence from human ligament anatomy, with five total ligaments that do not appear to have human analogues (Figure 7). In the superficial layer, these ligaments connected the radius and RCB (scaphoid), radius and ACB (pisiform), and the ulna and RCB (scaphoid). In the deep layer, one branching ligament connected the ICB (lunate) to the third and fourth carpal bones, and another attached to the radius and UCB (triquetrum). Superficially, analogues were found for the palmar distal intercarpals, scapholunate, lunotriquetral, ulnolunate, and ulnotriquetral ligaments in humans. In the deeper layer, we found analogues for the radioscaphocapitate, ulnocapitate, and triquetral-hamate-capitate ligaments.

There was significant overlap between porcine carpal ligaments and human ligaments important to stability, particularly on the dorsal side. Volar ligament anatomy in the YMP showed more divergence from human anatomy, as five ligaments we identified did not have human analogues. The presence of volar carpal ligaments that do not exist in humans could be due to functional differences in the joint between species. Pigs place more of their weight in the forelimb, potentially requiring greater stability than bipedal humans [35]. Alternatively, there is relatively low evolutionary pressure on any one specific carpal ligament – these differences in carpal ligaments could be variation due to phylogenetic distance between humans and pigs.

Appendix B – Additional Figures

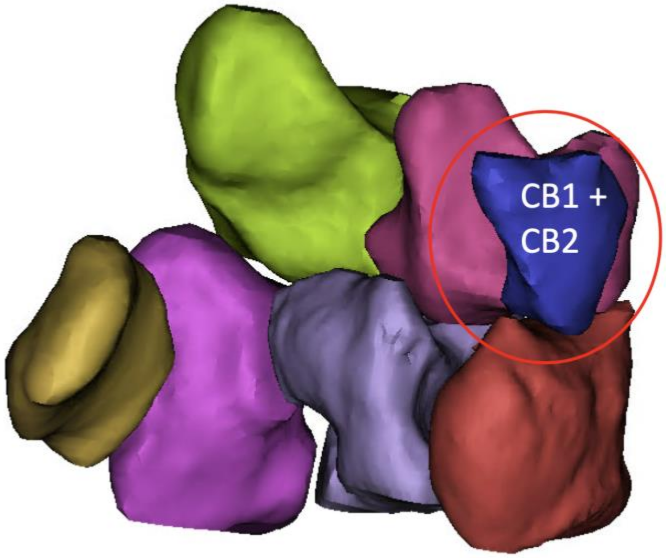

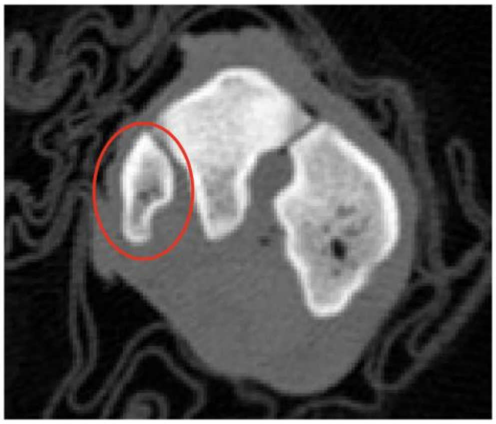

Figure B1. *Left*: A three-dimensional surface generated from the S13 CT scan, with CB1) and CB2 (blue) appearing to be fused. *Right*: Axial view of the S13 CT scan, showing complete fusion of CB1 and CB2 (circled).

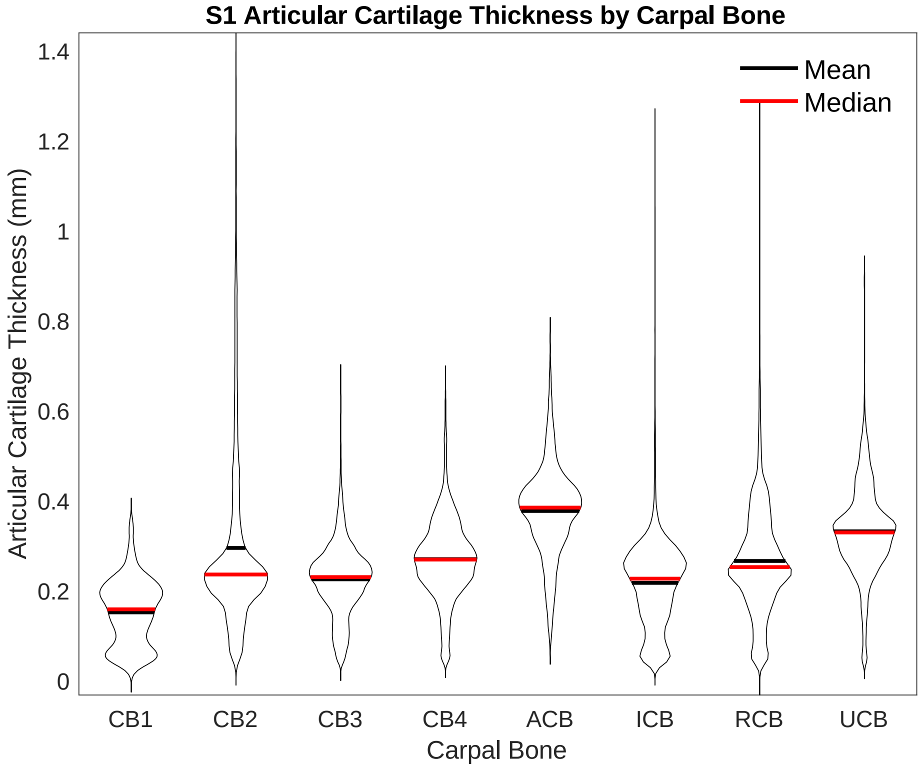

Figure B2. Articular cartilage thickness for each carpal bone in S1.